Temporal superoscillations of subterahertz coherent acoustic phonons

S. Brehm, A. V. Akimov, R. P. Campion, and A. J. Kent*
School of Physics and Astronomy, University of Nottingham, University Park, Nottingham NG7 2RD, United Kingdom

(Received 7 November 2019; revised manuscript received 7 February 2020; accepted 28 February 2020; published 6 April 2020)

We observe coherent acoustic phonon superoscillations at subterahertz frequencies. The superoscillations result from the interference of optically excited coherent longitudinal acoustic phonon modes in a GaAs/AlGaAs superlattice. The superoscillations are seen in local temporal regions and their frequency is up to 60% larger than the highest-frequency excited and detected phonon mode. Such superoscillatory phonon pulses may potentially be used for high-resolution acoustic measurement in strong scattering media.

DOI: 10.1103/PhysRevResearch.2.023009

I. INTRODUCTION

Coherent acoustic phonons with frequencies in the hundreds of gigahertz range, which are also known as acoustic nanowaves, are a powerful tool for investigating nanoscale objects with high temporal and spatial resolution. The established technique, known as picosecond acoustics, uses ultrafast (femtosecond) pulsed lasers to optically generate and detect coherent acoustic phonons with frequencies up to ~1 THz [1]. Such acoustic nanowaves can be used to probe the structural and mechanical properties of matter with subnanometer (sub-nm) axial resolution and submicrometer (sub-μm) transverse resolution [2]. Examples of the applications include studies of various nano-objects [3,4], interfaces [5], defects in solids [6], soft condensed matter [7], liquids [8], and biological matter (single cells) [9] (for a review see also [10]). Acoustic nanowaves have also been used for ultrafast control of photonic [11], electronic [12], and spintronic [13] devices.

Despite the successes of the picosecond acoustics technique, it suffers from a significant practical drawback: the strong attenuation and/or scattering, i.e., short mean free path, of high-frequency (more than approximately hundreds of gigahertz) phonons in many of the objects of interest. Causes of phonon attenuation and scattering include propagation through nonideal interfaces [14], e.g., between a stick-on optoacoustic transducer and the object under investigation; propagation in polycrystalline materials and crystals with a high defect density [15]; viscous damping [16]; natural isotope (point mass defect) scattering [17], which occurs even in perfect crystals. At ambient and room temperature, the mean free path of THz acoustic phonons in high-quality (semiconductor grade) crystals is only a few μm [18]. The result of these is that the mean free path decreases strongly with increasing phonon frequency with the net effect of imposing a bandwidth limit, restricting the highest frequency of the phonons that can be propagated in the system. This determines the highest phonon frequency that can be used in a picosecond acoustic measurement and hence the best resolution that could normally be obtained.

Bandwidth limitations also occur in measurements using electromagnetic waves and the search for ways to overcome these has led to renewed interest in the phenomenon of "superoscillation." Superoscillations occur in a band-limited function due the interference of a series of harmonic waves, Fourier series, with the appropriate amplitudes and phases. They are oscillations found in local temporal regions having rates arbitrarily higher than the highest-frequency Fourier component [19].

Superoscillations have relevance in all areas of physics where waves are superposed, e.g., in quantum mechanics [20]. It has also been proposed and demonstrated that superoscillations could be exploited to obtain improved optical resolution [21–24], ultrasonic lateral resolution [25], or radiofrequency measurement in bandwidth-limited systems [26]. The main problem with the practical application of superoscillations in many areas has been their small amplitude. However, advances in the sensitivity of measurements have prompted an increase in interest in the science and applications of the superoscillation phenomenon [27].

By analogy with their applications in optics, superoscillations could also offer the prospect of circumventing the bandwidth limitations in picosecond acoustics measurements. In practice, temporal acoustic superoscillations could be synthesized within the object under study by superposing a series of acoustic waves, all having frequencies below the bandwidth limits imposed by the acoustic attenuation and/or scattering mechanisms described above. These waves would possess a sufficiently long mean free path to propagate unimpeded to the point of interest within the object. Despite their relatively small amplitude, detection of the acoustic superoscillations is well within the capabilities of the asynchronous optical sampling (ASOPS) pump-probe measurement technique [28].

Here we use the picosecond acoustic technique to detect acoustic temporal superoscillations formed by interfering

*anthony.kent@nottingham.ac.uk

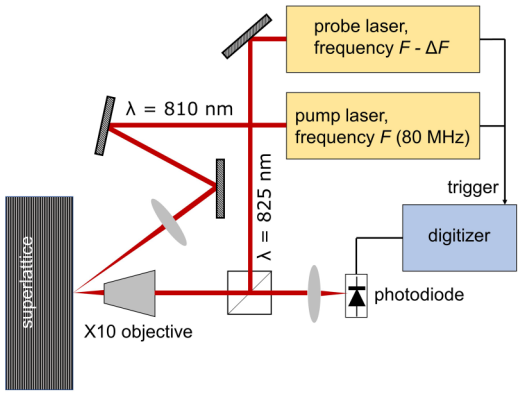

FIG. 1. ASOPS pump-probe setup using two 80-MHz femtosecond oscillators to excite and detect coherent phonon oscillations in a GaAs/AlGaAs superlattice (SL).

coherent phonon oscillations excited in a GaAs/AlGaAs superlattice (SL) by femtosecond optical pulses. We show that the observed superoscillatory features observed in local temporal regions are adequately modeled by summing the coherent phonon modes of the SL. This could open the door for future high-resolution acoustic measurement in strong scattering media.

II. METHODS

The experimental arrangement for the detection of coherent phonon superoscillations is shown in Fig. 1. The SL consists of 42 periods, each comprised of 13.3 nm of GaAs and 47.7 nm of $Al_{0.4}Ga_{0.6}As$, grown by molecular beam epitaxy on a GaAs substrate. The SL is excited by 810-nm-wavelength optical "pump" pulses of ∼100 fs duration and repetition rate 80 MHz from a femtosecond laser oscillator. The laser beam was focused to a spot of diameter ∼30 μm on the surface of the sample and had an average power of 100 mW, giving a fluence of 200 $\mu J/cm^2$. Absorption of the 810-nm radiation in the GaAs layers generates electron-hole pairs, and, through a combination of the thermoelastic and deformation potential effects, induces transient stresses in the structure. The spatially periodic nature of the induced stresses results in the generation of longitudinal-polarized coherent phonon modes within the SL having frequencies corresponding to the mini-Brillouin-zone center of the SL folded phonon dispersion, nc_s/d_{SL}, where c_s is the speed of sound in the SL, d_{SL} is the superlattice period equal to 61 nm, and n is an integer [29,30].

The phonons are detected using an optical "probe" pulse from a second 80-MHz, 100-fs femtosecond oscillator. The probe beam wavelength was 825 nm and the average power 10 mW. It was focused to a spot ∼5 microns in diameter on the surface of the sample and the reflected beam was detected by a photodiode. The strain associated with the coherent phonons leads to a modulation of the reflected beam intensity ΔR via the photoelastic effect [29,30]. In the chosen reflection geometry, the probe is sensitive to phonon modes having the wave vector twice the laser photon wave vector, $2k_{laser}$.

In the ASOPS [28] measurement, the frequencies of the pump and probe lasers were locked together with an offset of 800 or 400 Hz. The photodiode signal is amplified and recorded using a 125-MHz sample rate digitizer and signal averager. Using this setup and averaging over $\sim 10^7$ traces, we were able to detect changes in reflectance from the SL, $\Delta R/R \sim 10^{-8}$, with a signal to noise ratio of unity and a highest temporal resolution of 300 fs/point. The pump-probe pulse rms jitter of the ASOPS system was measured using a digital sampling oscilloscope to be 10 ps at an offset of 800 Hz. With a probe pulse repetition time of 12.5 ns and in a 1-ns-long measurement window, this corresponds to an instrumentation-limited detection bandwidth of about 1 THz, reducing to 500 GHz at an offset of 400 Hz.

III. RESULTS AND DISCUSSION

Figure 2 shows the signals obtained at room temperature, with a pump-probe laser frequency offset of 800 Hz, corresponding to a temporal resolution of 600 fs/point: the raw temporal trace [Fig. 2(a) upper panel] is dominated by the response due to the photoexcited electrons, but it is just possible to see the coherent phonon oscillations on the decaying tail. Subtraction of the electronic response and magnification reveals clearly the coherent phonon oscillations [Fig. 2(a) lower panel]. It is clear from the observed waveform that the signal results from the superposition of several coherent phonon harmonics, as is also apparent from the Fourier transform of the temporal data [Fig. 2(b)]. The observed frequencies correspond to the mini-Brillouin-zonecenter, $q = 0$, and edge, $q = 2k_{laser}$, phonon modes of the folded phonon dispersion. The latter are detected because, at the chosen probe wavelength, 825 nm, $2k_{laser} = \pi/d_{SL}$. In an ideal, infinite, SL the minizone center modes should not be detected in a reflection experiment and the minizone edge modes should not be generated. However, due to finite size effects, disorder, and optical absorption, both sets of modes are often generated and detected in pump-probe experiments [31]. It is clear from Fig. 2(b) that the coherent phonon signal is "band limited" with only the lowest seven or eight modes detected in the full temporal range. We can dismiss the possibility that this is due to bandwidth limitation of the ASOPS measurement caused by pulse jitter, which in our case is at least twice as high than the highest detected signal frequencies. The highest-frequency phonon modes that can be excited in the SL are ∼a few THz and related to the duration of the pump impulse which is ∼100 fs [32]. Decay of the excited high-frequency modes could be due to a number of reasons, which include damping of the phonons by extrinsic (phonon-defect) and intrinsic (phonon-phonon) scattering [33] and dephasing of the oscillations due to inhomogeneities in the SL [34].

Figure 3(a) shows a 200-ps-long section of the temporal trace of the coherent phonon oscillations recorded at the higher resolution of 300 fs/point (pump-probe laser frequency offset of 400 Hz). The 200-ps window begins at 250 ps after the start of the pump-probe signal. Highlighted regions, i–iii, show the temporal positions of three superoscillatory pulses, which are shown on an expanded scale in Fig. 3(c). The period of these single-cycle oscillations corresponds to a frequency of about 400 GHz, which exceeds the highest-frequency

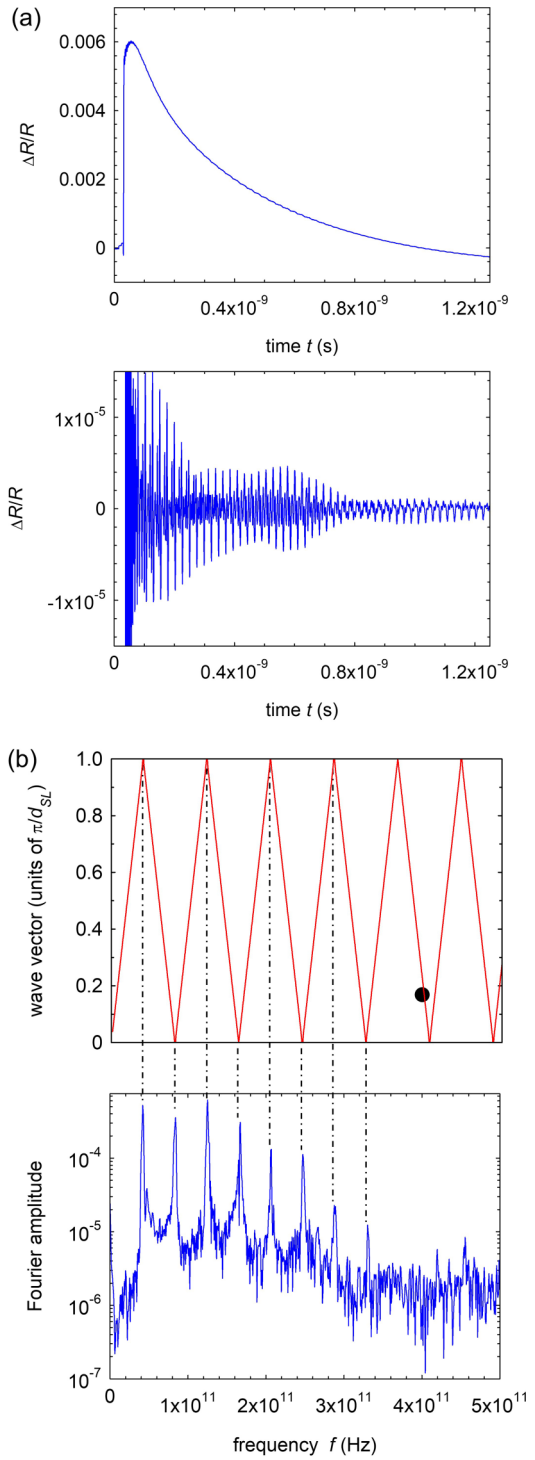

FIG. 2. Pump-probe measurements of coherent phonons in GaAs/AlGaAs SL: (a) (top panel) "raw" pump-probe signal with pump-probe laser offset frequency of 800 Hz (600 fs/point). The signal is dominated by the probe response to the electronic excitation, but coherent phonon oscillations are just visible on the decaying tail. After subtraction of the electronic background and magnification (lower panel), the coherent phonon oscillations are more clearly seen; (b) Fourier amplitude spectrum of the coherent phonon oscillations. Modes corresponding to the Brillouin minizone center (wave vector) and edge of the folded phonon dispersion of the SL (upper panel) are seen. The point marked on the dispersion plot indicates the frequency of the observed superoscillatory features.

component in the Fourier transform of the data [Fig. 3(b)]. The amplitude of the oscillations, $\Delta R/R \sim 10^{-7}$, which is an order of magnitude stronger than the rms amplitude of the noise floor following the averaging over 20 000 000 ASOPS traces. The frequency and amplitude of these oscillations are represented by the red bar in Fig. 3(b). The frequency is also represented by the point on the dispersion curve in Fig. 2(b), and clearly does not correspond to one of the mini-Brillouin-zone center or edge modes. That these features occur periodically in time is evidence that they are not due to random noise, and the following analysis indeed shows that these high-frequency features are superoscillatory in origin.

The solid red lines in Fig. 3(c) show the simulated temporal signal, $S(t)$, given by

$$s(t) = \sum_n A_n \sin(2\pi f_n t), \tag{1}$$

where A_n and f_n are, respectively, the amplitudes and frequencies of the Fourier components shown in Table I. These were extracted from the Fourier transform data shown in Fig. 3(b), which was taken in the same 200-ps temporal window, 250–450 ps. The signs of the amplitudes in Table I were obtained from the best fit to the experimental data. The simulated signal satisfactorily accounts for the temporal position, amplitude, and period of the superoscillatory features. Also shown by the dashed lines is the highest harmonic included in the simulations, $f = 248.9$ GHz. The frequency of the superoscillations, 400 GHz, exceeds the highest harmonic by about 60%.

In general, the superoscillating functions that result from the superposition of perfectly related harmonics, i.e., $f, 2f, 3f, \ldots$, tend to repeat periodically. In the case of the SL measured here, the modes are closely, but not perfectly harmonically related, which means the shape and frequency of the superoscillating functions are slightly different in each of the different localized temporal regions as seen in Fig. 3(c). When considering the experimental data, we also had to account for the fact that the various coherent phonon modes of the SL decay at different rates due to escape from the SL, dephasing due to inhomogeneity scattering, etc. [Fig. 2(a)]. Therefore, to be able to apply Eq. (1), while satisfactorily reproducing the data, we needed to restrict the analysis to within a 200-ps-wide window (250–450 ps) during which the amplitudes did not change significantly. This window included the temporal region in which the superoscillating features were observed. We used the mode amplitudes obtained by taking the Fourier transform in this window for simulating the superoscillations in Fig. 3(c). Furthermore, in some temporal regions outside of this window, the relative magnitudes of the harmonics were not appropriate for the observation of clear superoscillating functions. We note that the alternating sign of the amplitude (π phase shift) between the Brillouin minizone edge, having phonon wave vector $q = \pi/d_{\mathrm{SL}}$, and center, $q = 0$, modes in Table I is beneficial for obtaining superoscillations.

IV. CONCLUSION

In summary, using the ASOPS pump-probe measurement, we have observed features in the coherent phonon vibra-

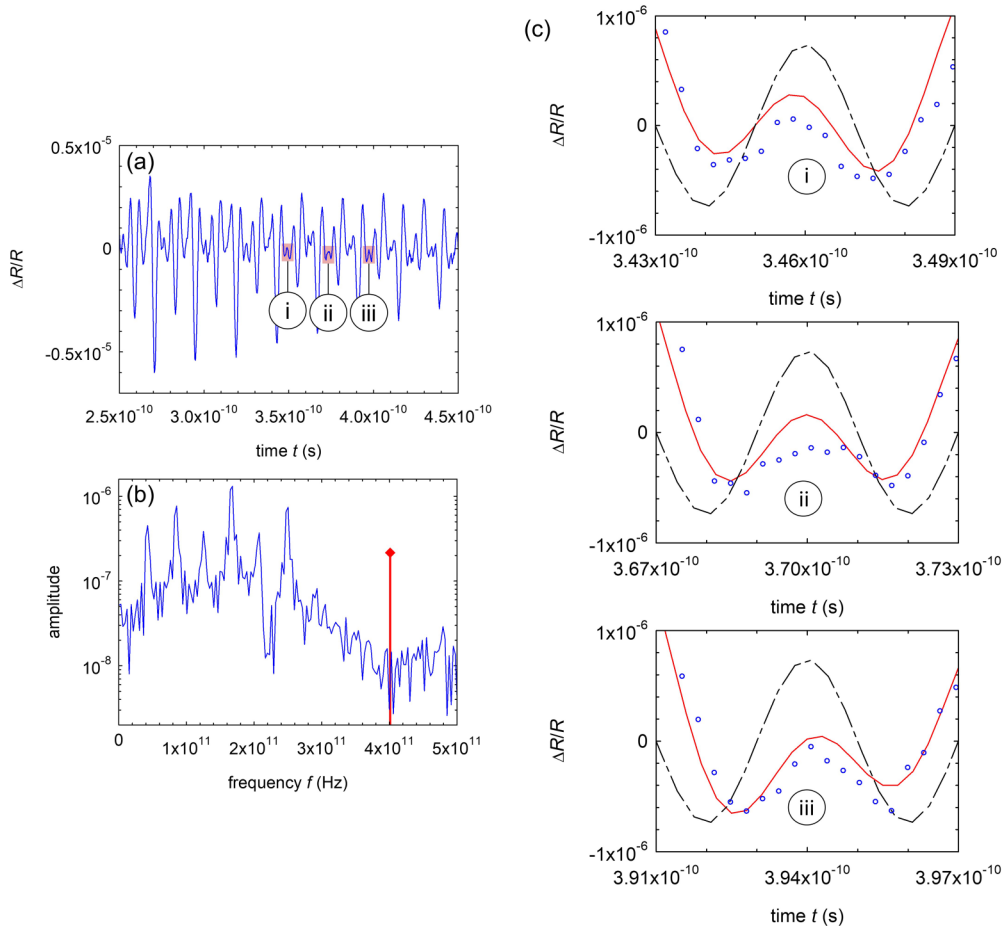

FIG. 3. Coherent phonon superoscillations: (a) temporal trace of the coherent phonon oscillations in a 200-ps window starting at 250 ps after the beginning of the pump-probe signal and recorded at a resolution of 300 fs/point (pump-probe laser offset frequency = 400 Hz). The three highlighted temporal regions, i – iii, indicate a few of the time windows where superoscillating functions are observed; (b) amplitude Fourier spectrum of the coherent phonon oscillations in (a); the red line represents the amplitude and frequency of the superoscillations; (c) temporal regions i – iii enlarged to show more clearly the observed superoscillations (blue circles). Also shown (solid red line) is the result of the simulation of the temporal trace by summing the Fourier components of the band-limited signal. The dashed-dotted line shows the highest-frequency Fourier component used in the summation.

tions of a GaAs/AlGaAs SL structure which oscillate faster than the highest Fourier component of the signal. We have shown that these features are superoscillatory in origin. The highest frequency of the observed superoscillations exceeded the highest-frequency phonon mode that was excited and detected by about 60%. This result points to a possible way of obtaining superresolution in picosecond acoustics measurements, considering, for example, the application of picosecond acoustics to measure the thickness of thin, nanometer films by a pulse-echo technique. Using superoscillatory pulses offers a higher resolution in a system where the bandwidth is limited by phonon scattering. This is analogous to the improved radar range resolution that had been reported in Ref. [26]. Superlattices could be ideal transducers for the generation of acoustic superoscillations in the sub-THz frequency range. The frequencies and amplitudes of the harmonics can be optimized by varying the SL period, the number of periods, and the thicknesses and compositions of the individual layers, as well as changing the wavelength of the pumping laser. Acoustic cavities could be created by growth of a thick layer inside or on top of the SL, which would give a more perfect relationship between the harmonic frequencies. More sophisticated acoustic transducers could be based on stacked multiple SLs, each designed to generate a phonon beam having a specific frequency, amplitude, and phase. If all the frequencies are lower than the bandwidth limit imposed by

TABLE I. Frequencies and amplitudes of the six most significant phonon modes in the temporal window 250– 450 ps, extracted from the data shown in Fig. 3(a) and used in Eq. (1) for the simulations of the superoscillatory features shown in Fig. 3(c).

Harmonic	Frequency (GHz)	Amplitude
1	41.9	-4.4×10^{-7}
2	84.9	7.4×10^{-7}
3	125.6	-3.7×10^{-7}
4	166.6	1.30×10^{-6}
5	207.0	-3.6×10^{-7}
6	248.9	7.5×10^{-7}

strongly frequency-dependent phonon scattering in the object of interest, these beams will propagate through the object and interfere with each other creating the superoscillations which may be probed by selecting the appropriate temporal region in the pump-probe trace.

ACKNOWLEDGMENTS

We acknowledge support from the EU Erasmus+ scheme, which funded S.B.'s placement in Nottingham to carry out this project.

[1] C. Thomsen, H. T. Grahn, H. J. Maris, and J. Tauc, Phys. Rev. B **34**, 4129 (1986).
[2] K. Lin, C. Lai, C. Pan, J. Chyi, J. Shi, S. Sun, C. Chang, and C. Sun, Nat. Nanotechnol. **2**, 704 (2007).
[3] T. Dehoux, O. B. Wright, R. Li Voti, and V. E. Gusev, Phys. Rev. B **80**, 235409 (2009).
[4] V. Juvé, A. Crut, P. Maioli, M. Pellarin, M. Broyer, N. Del Fatti, and F. Vallée, Nano Lett. **10**, 1853 (2010).
[5] J. D. G. Greener, E. de Lima Savi, A. V. Akimov, S. Raetz, Z. Kudrynskyi, Z. D. Kovalyuk, N. Chigarev, A. Kent, A. Patané, and V. Gusev, ACS Nano **13**, 11530 (2019).
[6] A. Steigerwald, Y. Xu, J. Qi, J. Gregory, X. Liu, J. K. Furdyna, K. Varga, A. B. Hmelo, G. Lüpke, L. C. Feldman, and N. Tolk, Appl. Phys. Lett. **94**, 111910 (2009).
[7] H. Kim, Y. Cang, E. Kang, B. Graczykowski, M. Secchi, M. Montagna, A. D. Priestley, E. M. Furst, and G. Fytas, Nat. Commun. **9**, 2918 (2018).
[8] A. A. Maznev, K. J. Manke, C. Klieber, K. A. Nelson, S. H. Baek, and C. B. Eom, Opt. Lett. **36**, 2925 (2011).
[9] T. Dehoux and B. Audoin, J. Appl. Phys. **112**, 124702 (2012).
[10] B. Peronne and B. Perrin, Ultrasonics **56**, 1 (2015).
[11] C. Brüggemann, A. V. Akimov, A. V. Scherbakov, M. Bombeck, C. Schneider, S. Höfling, A. Forchel, D. R. Yakovlev, and M. Bayer, Nat. Photonics **6**, 30 (2012).
[12] E. S. K. Young, A. V. Akimov, M. Henini, L. Eaves, and A. J. Kent, Phys. Rev. Lett. **108**, 226601 (2012).
[13] J. V. Jäger, A. V. Scherbakov, T. L. Linnik, D. R. Yakovlev, M. Wang, P. Wadley, V. Holy, S. A. Cavill, A. V. Akimov, A. W. Rushforth, and M. Bayer, Appl. Phys. Lett. **103**, 032409 (2013).
[14] E. T. Swartz and R. O. Pohl, Appl. Phys. Lett. **51**, 2200 (1987).
[15] C. T. Walker and R. O. Pohl, Phys. Rev. **131**, 1433 (1963).
[16] W. P. Mason, J. Acoust. Soc. Am. **32**, 458 (1960).
[17] P. G. Klemens, in *Solid State Physics*, edited by F. Seitz and D. Turnbull (Academic, New York, 1958), Vol. 7.
[18] R. Legrand, A. Huynh, B. Jusserand, B. Perrin, and A. Lemaitre, Phys. Rev. B **93**, 184304 (2016).
[19] M. V. Berry, in *Quantum Coherence and Reality: In Celebration of the 60th Birthday of Yakir Aharonov*, edited by J. S. Anandan and J. L. Safko (World Scientific, Singapore, 1994), pp. 55–65.
[20] Y. Aharonov, J. Anandan, S. Popescu, and L. Vaidman, Phys. Rev. Lett. **64**, 2965 (1990).
[21] M. V. Berry and S. Popescu, J. Phys. A **39**, 6965 (2006).
[22] F. M. Huang, T. S. Kao, V. A. Fedotov, Y. Chen, and N. I. Zheludev, Nano Lett. **8**, 2469 (2008).
[23] N. I. Zheludev, Nat. Mater. **7**, 420 (2008).
[24] Y. Eliezer, L. Hareli, L. Lobachinsky, S. Froim, and A. Bahabad, Phys. Rev. Lett. **119**, 043903 (2017).
[25] Y.-X. Shen, Y.-G. Peng, F. Cai, K. Huang, D.-G. Zhao, C.-W. Qiu, H. Zheng, and X.-F. Zhu, Nat. Commun. **10**, 3411 (2019).
[26] A. M. Wong and G. V. Eleftheriades, IEEE Microwave Wireless Compon. Lett. **22**, 147 (2012).
[27] M. Berry, N. Zheludev, Y. Aharonov, F. Colombo, I. Sabadini, D. C. Struppa, J. Tollaksen, E. T. F. Rogers, F. Qin, M. Hong *et al.*, J. Opt. **21**, 053002 (2019).
[28] A. Bartels, F. Hudert, C. Janke, T. Dekorsy, and K. Köhler, Appl. Phys. Lett. **88**, 041117 (2006).
[29] A. Yamamoto, T. Mishina, Y. Masumoto, and M. Nakayama, Phys. Rev. Lett. **73**, 740 (1994).
[30] A. Bartels, T. Dekorsy, H. Kurz, and K. Köhler, Phys. Rev. Lett. **82**, 1044 (1999).
[31] A. Huynh, B. Perrin, and A. Lemaître, Ultrasonics **56**, 66 (2015).
[32] M. F. Pascual-Winter, A. Fainstein, B. Jusserand, B. Perrin, and A. Lemaître, Phys. Rev. B **85**, 235443 (2012).
[33] A. A. Maznev, F. Hofmann, A. Jandl, K. Esfarjani, M. T. Bulsara, E. A. Fitzgerald, G. Chen, and K. A. Nelson, Appl. Phys. Lett. **102**, 041901 (2013).
[34] G. Rozas, M. F. Pascual Winter, B. Jusserand, A. Fainstein, B. Perrin, E. Semenova, and A. Lemaître, Phys. Rev. Lett. **102**, 015502 (2009).